# Final Report for Grant FA2386-09-1-4035 (AOARD 094035)

*Date: November 15, 2010*

## <Research Title>

## "Hybrid Inorganic/Organic Photovoltaics: Translating Fundamental Nanostructure Research to Enhanced Solar Conversion Efficiency"

## (Period of Performance: Oct. 12, 2009-Oct. 11, 2010)


**Key Researcher (PI):**

Prof. Kwang-Sup Lee
Department of Advanced Materials, Hannam University
461-6 Jeonmin-Dong, Yuseong-Gu, Daejeon 305-811, South Korea
Phone: +82-42-629-8857, FAX: +82-42-629-8854
E-mail address: kslee@hnu.kr

**Joint Researchers**

Prof. Alex N. Cartwright, Institute for Laser, Photonics and Biophotonics,
University at Buffalo, SUNY, Buffalo, NY 14260, USA
Phone: +1-716-645-2422 (Ext.1205), Fax: +1-716-645-3656
E-mail: anc@buffalo.edu

Prof. Paras N. Prasad, Institute for Laser, Photonics and Biophotonics,
University at Buffalo, SUNY, Buffalo, NY 14260, USA
E-mail: pnprasad@buffalo.edu

Prof. Sailing He
Dept. of Optical Engineering, Zhejiang Univ., Yu-Quan, China
E-mail: sailing@zju.edu.cn


**AOARD Program Manager** Dr. Thomas Erstfeld
**AFOSR Program Manager** Dr. Charles Lee

# Report Documentation Page

*Form Approved*
*OMB No. 0704-0188*



| 1. REPORT DATE | 2. REPORT TYPE | 3. DATES COVERED |
|---|---|---|
| **05 JAN 2011** | **Final** | **01-07-2009 to 31-10-2010** |

4. TITLE AND SUBTITLE
**Hybrid Inorganic/Organic Photovoltaics: Translating Fundamental Nanostructure Research to Enhanced Solar Conversion Efficiency**

5a. CONTRACT NUMBER
**FA23860914035**

5b. GRANT NUMBER

5c. PROGRAM ELEMENT NUMBER

6. AUTHOR(S)
**Kwang-Sup Lee**

5d. PROJECT NUMBER

5e. TASK NUMBER

5f. WORK UNIT NUMBER

7. PERFORMING ORGANIZATION NAME(S) AND ADDRESS(ES)
**Hannam University,461-6 Jeonmin-Dong, Yuseong-Gu,Daejeon 306-811,Korea (South),NA,NA**

8. PERFORMING ORGANIZATION REPORT NUMBER
**N/A**

9. SPONSORING/MONITORING AGENCY NAME(S) AND ADDRESS(ES)
**AOARD, UNIT 45002, APO, AP, 96338-5002**

10. SPONSOR/MONITOR'S ACRONYM(S)
**AOARD**

11. SPONSOR/MONITOR'S REPORT NUMBER(S)
**AOARD-094035**

12. DISTRIBUTION/AVAILABILITY STATEMENT
**Approved for public release; distribution unlimited**

13. SUPPLEMENTARY NOTES

14. ABSTRACT
**This is the report of a research project to improve the efficiency of organic photovoltaics through material and device design innovations.**

15. SUBJECT TERMS
**Solar Cells, Polymer Chemistry**

| 16. SECURITY CLASSIFICATION OF: | | | 17. LIMITATION OF ABSTRACT | 18. NUMBER OF PAGES | 19a. NAME OF RESPONSIBLE PERSON |
|---|---|---|---|---|---|
| a. REPORT | b. ABSTRACT | c. THIS PAGE | | | |
| **unclassified** | **unclassified** | **unclassified** | **Same as Report (SAR)** | **16** | |

## 1. Abstract

Improving the efficiency of organic photovoltaics through material and device design innovations is a prolific field in alternative energy research. The purpose of our research is to develop key concepts that will enable new design criteria for organic photovoltaic (PV) cells based on polymeric nanocomposites, which are expected to produce large enhancement in power conversion efficiency. In this report for the third and final year we report the microstructure tuning of nanoparticle films by making them photopatternable, development of fullerene derivatives which are highly efficient n-type semiconductor, design and synthesis of low bandgap polymers, the improvement of solar cells by local surface plasmon resonance enhancement of light, and achieving higher efficiency in quatumn dot (QD)-polymer solar cells by ligand exchange of QD ligands.

## 2. Introduction

The features of polymer based photovoltaic devices such as flexibility, light-weight, radiation resistance and ease of use for large area structural applications suit them enormously for applications in military aircraft, aerospace applications and optoelectronic devices. However the current pace at purely organic or polymer-based photovoltaics is progressing would only lead to incremental increase in the efficiencies of these devices due to the inefficient harvesting of the UV and IR-photons, as well as the limited carrier mobility in polymers. Our research involve the hybrid approach in which inorganic materials like quantum dot (QD), carbon nanotubes (CNTs) and fullerene derivatives are combined with organic components to achieve efficient bulk heterojunction solar cells. We look at the materials, their interfaces and the resultant transport mechanisms in the devices to understand and improve our design of devices as well materials.

In this project we propose new approaches for highly efficient organic solar cells by applying a unique combination of our expertise in (i) synthesis of inorganic nanostructures, (ii) integration of polymeric nanocomposites with CNTs or polypyrrole nanotubes (PPyNTs) functionalized with UV-, Vis-, IR-active QDs by chemical modification, (iii) surface modification of QDs for efficient patterning of multilayer PV devices, (iv) synthesis of various $C_{60}$ derivatives coupled with thiophene oligomers, (v) synthesis of low band gap polymeric materials, and (vi) gold nanorod generated surface Plasmon enhanced light harvesting in hybrid photovoltaics.

**In the first year (Oct. 12, 2007-Oct.11, 2008)** we accomplished synthesis of quantum dots with and without core-shells and studied their optical properties. We also successfully functionalized single wall carbon nanotubes (SWCNT) with CdSe QDs and polypyrrole nanotubes (PPyNTs) with PbSe QDs to study the effectiveness of nanotubes to separate the carriers generated by the QDs on photoexcitation. The first year also involved the design and synthesis of low-bandgap polymers and fullerene derivatives to be used in bulk heterojunction solar cells where the former is the electron donor and the latter the electron acceptor.

**During the second year (Oct. 12, 2008-Oct. 11, 2009)** we accomplished successful synthesis and application of photopatternable t-BOK ligand protected CdSe, CdTe and PbSe QDs for application as patterend bulk heterojuntions. The effect of hole blocking PEDOT:PSS layer in increasing the effectiveness of hybrid inforganic-organic solar cells were also investigated during this period. On the material front this period involved the development of very low- bandgap polymers, we also studied C60 derivatives substituted with thiophene based moieties. One of the derivatives were found to be a record n-type fullerene based organic

semiconductor with performance about an order of magnitude greater than the widely accepted standard PCBM.

**The goal of the third year (Oct. 12, 2009-Oct.11, 2010)** of this project involve

- *Enhanced broadband energy harvesting using engineered and surface functionalized semiconductor nanocrystals (quantum dots) of various sizes, shapes and compositions (HNU-UB-ZJU).*
- *Introduction of conjugated linker molecules for interconnection of inorganic nanocrystals and nanotubes for improved electron transfer between these nanoscale components (HNU-UB).*
- *Enhanced exciton dissociation and minimized recombination via bandgap-engineered multi-component hybrid nanocrystals through control of interfacial chemistry and linkage to other components (UB-HNU-ZJU)).*
- *Energy harvesting of the NIR region of the solar spectrum by the use of low band gap polymers coupled with electron accepting C60 derivatives (HNU-UB).*
- *Efficient charge transfer in polymeric devices through donor-acceptor type systems (HNU-UB).*
- *Use of nanoparticles acting as antennas to increase light harvesting (ZJU-HNU).*
- *Development and use of patternable quantum dots and application of generated patterns as light harvesting domains(HNU-UB).*

**Scheme 1. Research approaches for improved efficiency of hybrid solar cells.**

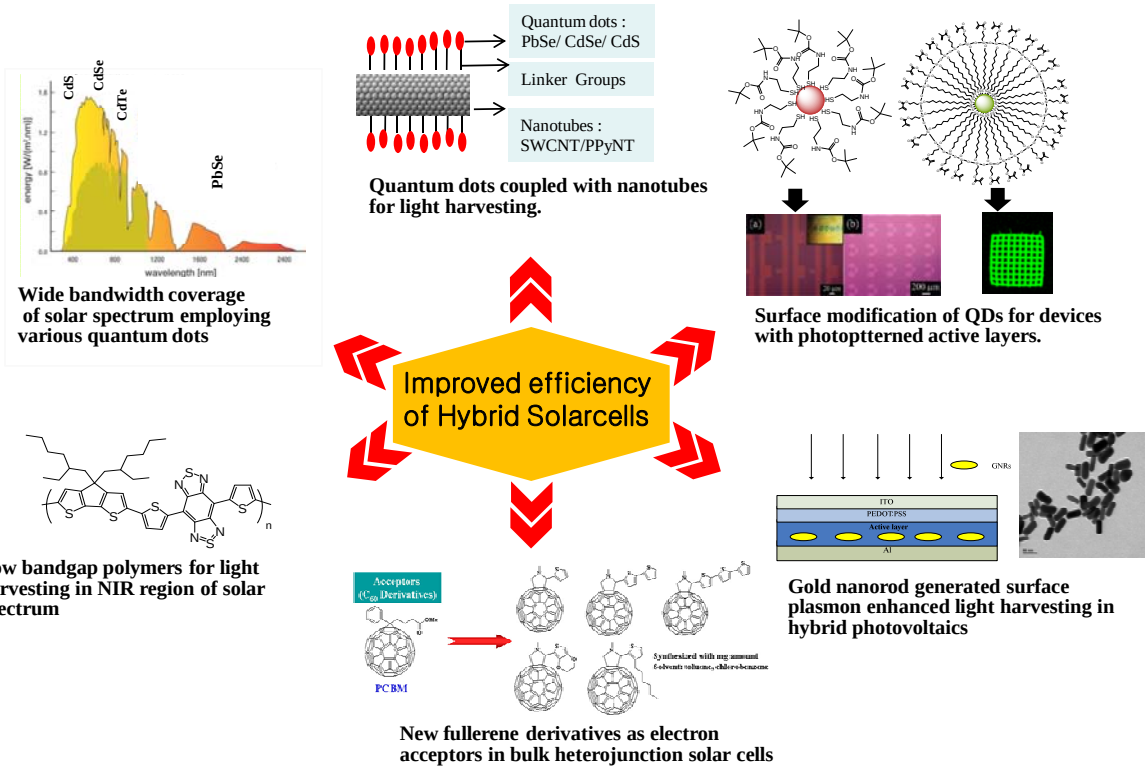

## 3. Results and Discussion

### 1) Photopatternable quantum dots (QDs)

Earlier we had reported the design and synthesis of patternable quantum dots involving light cleavable *t*-BOK units as active species. We have also designed and synthesized quantum dots containing photopatternable methacrylate corona. In order to investigate the role of ligands in the optical properties of coreshell CdSe@ZnS quantum dots, we synthesized quantum dots stabilized by a series of ligands seen in **Figure 1**. This series constitutes first of QDs stabilized with mercaptoundecyl ligands, the second one constitute of mercaptoundecanol as the first ligand which is further complexed with hexyltrimethoxy silane to form a ligand configuration with an inner siloxane layer and an alkyl corona around the QDs, the third type of QDs constituted an inner siloxane layer as well as an outer polymerizable corona of methacrylate groups. Films of all three types of QDs showed enhancement of photoluminescence properties when they are UV irradiated. The latter two types of QDs showed dramatic enhancement in their photoluminescence properties with increase of PL intensities from 1-1.6 orders of magnitude. Comparison of the textures of these QD films by transmission electron microscopy (TEM) showed a quasi-ordering effect in the acrylate terminated QDs after irradiation. Thus photoirradiation of the patternable QDs become a way to manipulate the microstructure of the QD films. The comparison of TEM images of microstructures of the three different types of QDs is can be seen in **Figure 2**.

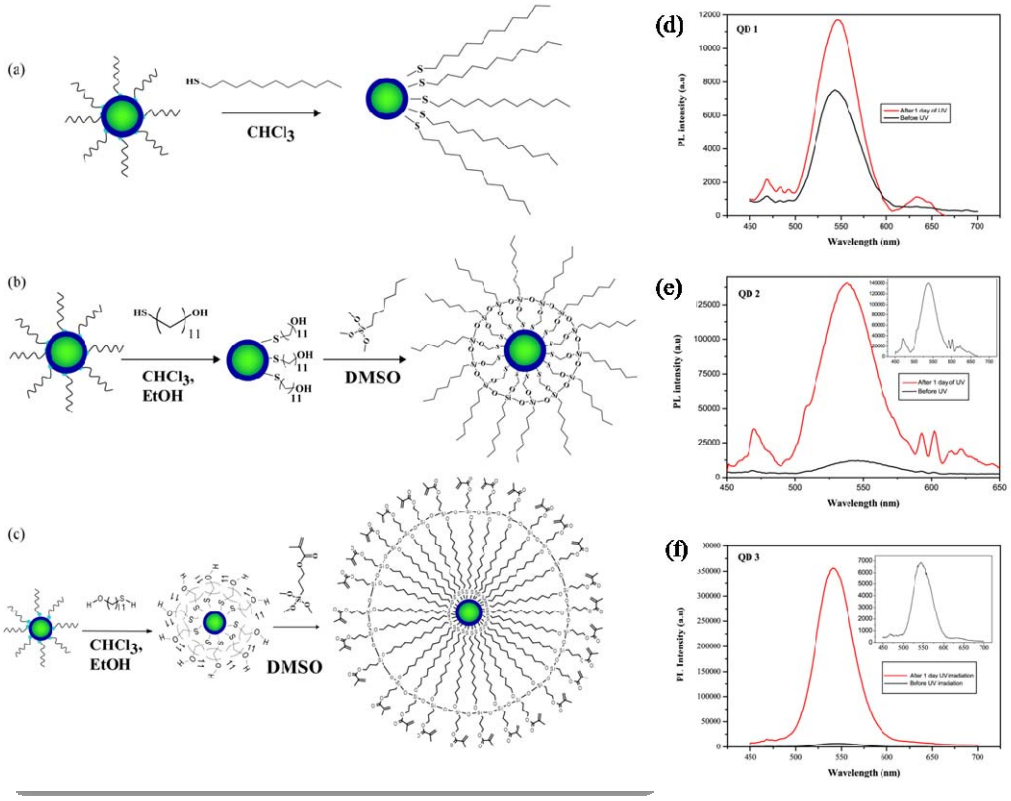


**Figure 1.** Shows the three types of quantum dots synthesized for this study, (a) the alkyl-terminated (b) siloxane inner layer containing alkyl-terminated, (c) photpatternable QD with siloxane inner layer and the photopolymerizable methacrylate corona. (d)-(f) Effect of irradiation on PL spectra. (d) The PL spectra of QDs with alkyl corona before and after UV irradiation for one day, (e) the photoluminescence siloxane inner layer containing alkyl-terminated QDs before and after UV irradiation under same conditions, (f) The large enhancement in PL of the photopatternable QD film after UV exposure compared with that before irradiation.

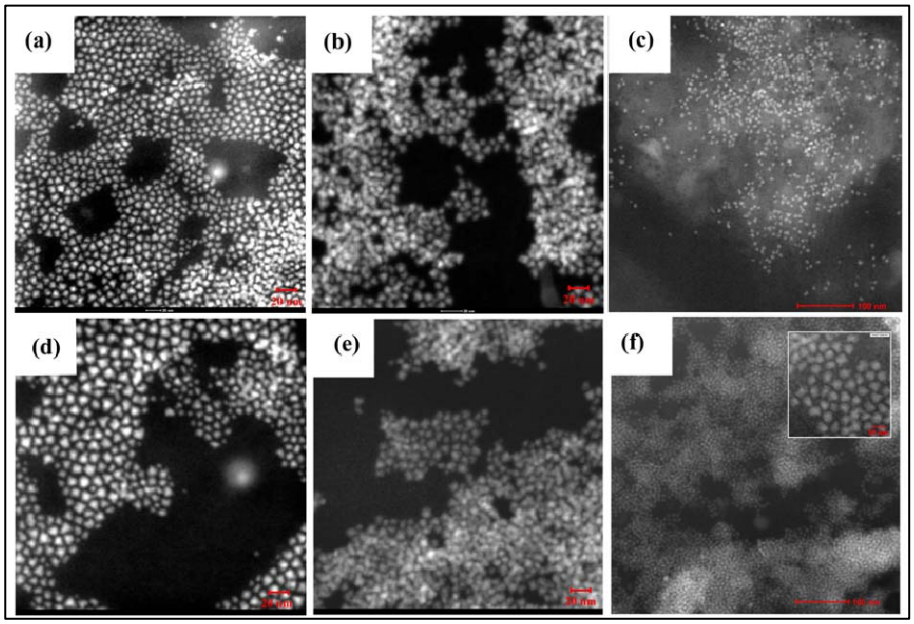


**Figure 2.** (a), (b), and (c) Respective TEM images of alkyl-terminated QDs, siloxane-coated alkyl-terminated QDs, and the photopatternable QDs before UV irradiation; the scale bar in (a) and (b) is 20 nm while that in (c) is 100 nm. (d) The TEM image of alkyl-terminated QDs after UV irradiation (scale20 nm). (e) TEM image of siloxane-coated alkyl-terminated QDs after irradiation (scale 20 nm). (f) photopatternable QDs after irradiation (scale 100 nm). The inset in (f) shows a closer looks at the cross-linked QDs (scale 10 nm).

The inherent properties of photopolymerizable QDs such as their stability, PL, and ease of solution processability, make them suitable materials for the active layers of electroluminescent devices. The first example of a QD-based light-emitting diode (QD LED) was a device based on an indium-tin-oxide (ITO) supported hole-transporting poly(phenylene vinylene) (PPV) film interfaced to a capped CdSe-nanoparticle film with Mg top electrode. To evaluate the potential of this material, we fabricated electroluminescent devices in which the active layer was a spin-cast film of photofunctionalized QDs. In addition, to evaluate the role of photordering in the device performance, we carried out studies on devices with and without exposure of their active layer to UV light. The structure and characteristics of these devices are summarized **in Figure 3(a) and (b).** The EL properties of the QD-LED devices were examined using a five-layer LED-device configuration, as shown in the inset of **Figure 3(a)**, where the conducting polymer PEDOT was used as the hole-injecting layer. The thickness of the ITO anode was 150 nm, and the sheet resistance was 10 Ω/□. The hole-injection layers were spin-coated to give 55 nm-thick films on top of the ITO glass after surface treatment (for one minute) with oxygen plasma. Subsequently, the surfaces were baked in air at 110°C for 2 hours. An interlayer was spin-coated (the spin-coating step was 500 rpm/5 s-2000 rpm/50 s-500 rpm/5s) on the HIL(hole-injection layer)layers, using TFB to obtain a 20 nm-thick film, and then baked at 180°C for 30 min and subsequently at 90°C for one minute. Then, a 30 mg/ml nanocrystal solution was spin-coated (the spin-coating step was 500 rpm/5s-3000 rpm/ 50s-500 rpm/5s) on top of the interlayer and baked at 90 °C for one minute. Subsequently, a 30 nm-thick tris(8-hydroxyquinoline)-aluminum(III) ($Alq_3$) film was thermally deposited onto the QD layers, thereby serving as electron transport layer (ETL). LiF (1 nm) and Al (100 nm) layers were sequentially deposited (under vacuum; $P<10^{-6}$ Torr) onto the ETL. Finally, the QD-LED unit devices were encapsulated with a cover glass for characterization in the glove box using a UV-curable epoxy resin and a CaO getter. The current–voltage–luminescence (*I–V–L*) characteristics of the devices

were obtained using a Keithley 238 unit and a Photo Research PR650 spectrophotometer. The image of a working device is given in one of the insets in **Figure 3(b).**

In green electroluminescent devices involving $Alq_3$, it is usually difficult to distinguish between the electroluminescence of the green active component and that of $Alq_3$. In the case of the present device, we could readily distinguish the electroluminescence associated with green QDs because of the distinctive fingerprints of the QD and $Alq_3$ emissions, as given in CIE coordinates in the inset of Figure 4(c). From the electroluminescence (EL) spectrum, it could be clearly inferred that light emission was generated from the QDs and not from $Alq_3$ [see Figure 4(b)]. The device whose active layer was exposed to UV light showed a strong green emission with a quite low turn-on voltage (i.e., the voltage needed to achieve a brightness of 1 cd/m$^2$) at 4.8 V. The luminance reached a value of 4384 cd/m$^2$ at a drive voltage of 13 V and a current density of 182 mA/cm$^2$, corresponding to an efficiency of 2.40 cd/A and a luminosity of 0.58 lm/W. The maximum external quantum efficiency was 0.62% at 588 cd/m$^2$ (with a bias of 9.5 V). It is well known that conjugated polymers absorbing visible light degrade upon intense irradiation. The photoinduced degradation of conjugated polymers is accelerated in the presence of oxygen. Photo-oxidation severely affects the molecular structures of poly(3,4-ethylene dioxythiophene):poly(styrenesulfonate) (PEDOT:PSS) and poly[(9,9-dioctylfluorenyl-2,7-diyl)-co-(4,4′-(N-(4-sec-butylphenyl))diphenylamine) (TFB) upon UV exposure after coating photosensitive QDs as the emitting layer. In the case of the device whose active layer was not exposed to UV radiation, the luminance reached a value of 2996 cd/m$^2$ at a drive voltage of 13 V and a current density of 191 mA/cm$^2$; this corresponds to an efficiency of 1.57 cd/A and a luminosity of 0.38 lm/W. The maximum external quantum efficiency is 0.53% at 703 cd/m$^2$ and a bias of 10.0 V. Although the photo-oxidation of the conducting polymer affects the device performance, the photoinduced nanomatrix array composed of QDs enhances the EL efficiency by up to 52% when compared to the efficiency of the devices without UV exposure.

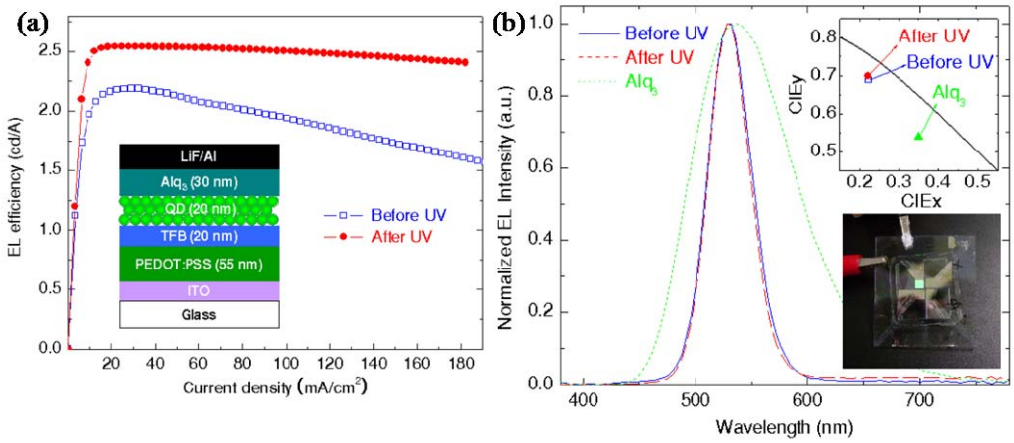


**Figure 3.** (a) Structure and performance of electroluminescent devices fabricated with and without photocured green-quantum-dot layer as the active component. The graph shows the EL efficiency vs current density characteristic of the devices before and after UV exposure, and the inset shows the structure of the device. The cured device shows maximum external quantum efficiency (EQE) of 0.62% at 588 cd/m2 whereas the uncured device shows an EQE of 0.53% at 703 cd/m2. (c) Comparison of the green emissions from the quantum dot sand AlQ3. Because of the distinctive signature of both compounds, they are easily recognizable in the CIE coordinate system given in the inset. A second inset shows an image of the working device.

Patterened QD interfaces can be used as donors in bulk heterojunction solar cells. Achivement of high resolution patterns of dimensions of the order of the diffusion length of excitons we could improve the performance of bulk heterojunction solar cells. The interesting enhancement of optical properties seen in photocured films could also contribute to an increase

in efficiency of the photovoltaic cells if they are combined with suitable acceptor materials and polymers.

**2) Increased open-circuit voltage in bulk-heterojunction solar cells using a C60 derivative**

Increasing the photoconversion efficiency in bulk heterojunction (BHJ) solar cells has been the goal of many groups that are working on this topic. There are two main strategies for increasing the PCE.

(i) Increasing the short circuit current ($J_{sc}$), by synthesis of low band gap polymers that absorb light extending into the red or infrared spectral range.

(ii) Obtaining higher open circuit voltage ($V_{oc}$) by lowering the energy of the highest occupied molecular orbital (HOMO) of the semiconducting polymer and/or raising the energy of the lowest unoccupied molecular orbital (LUMO) of fullerene acceptor.

In BHJ solar cells, $V_{oc}$ is determined by the difference between the HOMO energy of the semiconducting polymer and LUMO energy of the fullerene derivative.

Many fullerene derivatives have been synthesized and tested in BHJ solar cells. However, [6,6]-phenyl-$C_{61}$-butyric acid methyl ester ($PC_{60}BM$) continues to be the best known acceptor. In BHJ solar cells with low hand-gap polymers, $V_{oc}$ is limited by the LUMO energy of $PC_{60}BM$. Although some $PC_{60}BM$ analogues have succeeded in demonstrating higher LUMO values, the performances in solar cells are poor because of their poor charge transport properties.

We have designed and synthesized $C_{60}$-fused *N*-methyl-2-(3-hexylthiophen-2-yl)pyrolidine ($C_{60}$-TH-Hx) shows high electron mobility of $1.4 \sim 1.8 \times 10^{-2}$ $cm^2V^{-1}s^{-1}$ in n-type FETs; i.e. one order of magnitude higher than that of $PC_{60}BM$. Interestingly, the LUMO energy of $C_{60}$-TH-Hx is 3.8 eV, well above that of $PC_{60}BM$.[13] Therefore, higher $V_{oc}$ is expected from BHJ solar cells fabricated with $C_{60}$-TH-Hx as the acceptor. We have investigated the photovoltaic performance of $C_{60}$-TH-Hx as an acceptor material in BHJ solar cell. The low band gap polymer, poly[(4,4'-bis(2-ethylhexyl)dithiene[3,2-b:2',3'-d]silole)-2,6-diyl-alt-(4,7-bis(2-thienyl)-2,1,3-benzothia-diazole)-5,5'-diyl], (Si-PCPDTBT), was used as the donor polymer. Higher $V_{oc}$ (0.675 V) and PCE = 4 % were obtained. The result implies that $C_{60}$-TH-Hx is a promising acceptor for high performance BHJ solar cells and supports the strategy of synthesis of fullerene derivatives for BHJ solar cells. Summarized in **Figure 4(a)** are the structures of $PC_{60}BM$, $C_{60}$-TH-Hx and Si-PCPDTBT. The energy level diagram of the solar cell devices fabricated is given in **Figure 4(b)**. The absorption spectrum of $PC_{60}BM$, $C_{60}$-TH-Hx and Si-PCPDTBT is given in **Figure 4(c)**.

To find the optimum blend ratio, devices were prepared and tested with various mixture ratios (1:1, 1:2, and 1:4, w/w). As shown in **Figure 5(a)**, the performance depends on the amount of $C_{60}$-TH-Hx. The 1:1 ratio Si-PCPDTBT:$C_{60}$-TH-Hx yields PCE = 1.514 % with $J_{sc}$ = 5.084 mA/$cm^2$, $V_{oc}$ = 0.608, FF = 0.49, while device with 1:2 ratio resulted PCE = 4.023 % with $J_{sc}$ = 10.62 mA/$cm^2$, $V_{oc}$ = 0.675 V, FF = 0.561. In the case of 1:4 ratio solar cell, the performance was decreased in PCE = 3.278 % with $J_{sc}$ = 8.922 mA/$cm^2$, $V_{oc}$ = 0.644 V, FF = 0.571. We conclude that the optimum Si-PCPDTBT:$C_{60}$-TH-Hx mixture ratio is 1:2. This result is similar with the optimum condition of Si-PCPDTBT:$PC_{60}BM$.

The absorption spectra of $PC_{60}BM$ and $C_{60}$-TH-Hx show strong absorptivity below 550 nm. Between 400 nm and 550 nm, the absorption coefficient of $C_{60}$-TH-Hx is larger than that of $PC_{60}BM$. In the short wavelength region below 400 nm, $PC_{60}BM$ exhibits the well-known resolved peaks. However, for the $C_{60}$-TH-Hx, it is difficult to resolve these peaks in the same wavelength region. This indicates that the change of functional group on fullerene induces the increase of absorption in the visible range and affects on the electronic structure of the fullerene. The direct comparison of J-V characteristics between the Si-PCPDTBT:$C_{60}$-TH-Hx solar cell and Si-PCPDTBT:$PC_{60}BM$ solar cell is shown in **Figure 5(b)**. The solar cell with $PC_{60}BM$ yields the PCE = 4.038 % with $J_{sc}$ = 12.21 mA/$cm^2$, $V_{oc}$ = 0.594 V, and *FF* = 0.557. This result

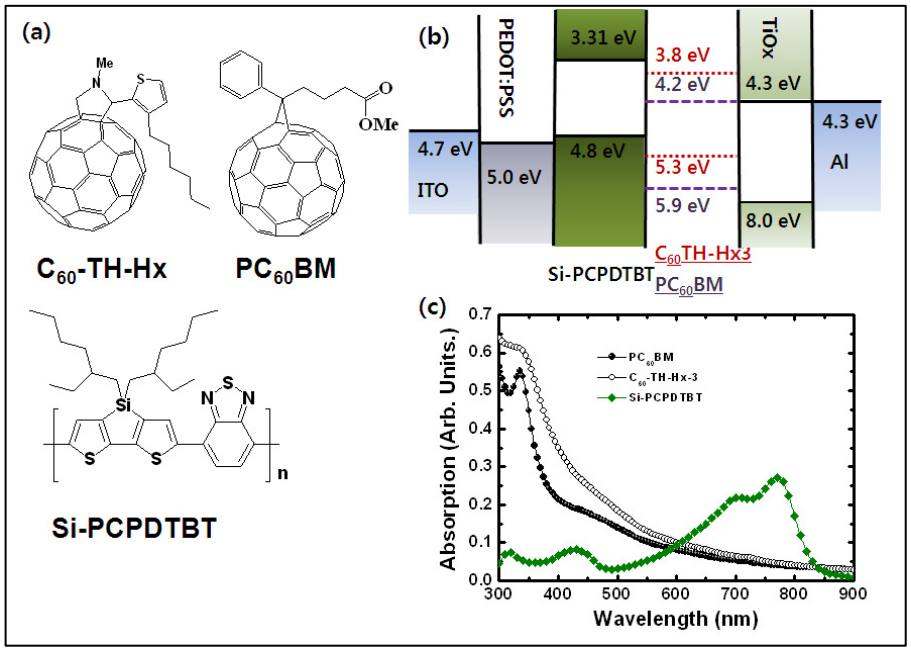


**Figure 4.** (a) Molecular structures of $C_{60}$-TH-Hx, $PC_{60}BM$, and Si-PCPDTBT, (b) Energy level diagrams of the BHJ components and (c) Absorption spectra of $PC_{60}BM$, $C_{60}$-TH-Hx and Si-PCPDTBT.

is consistent with that in the literature. Although Si-PCPDTBT:$C_{60}$-TH-Hx solar cell shows a slight decrease of (value) in $J_{sc}$, and PCE ≈ 4%; because of the larger $V_{oc}$ (0.675 V) and *FF* (0.561). Particularly, the $V_{oc}$ increases approximately 0.1 V. From the energy level diagram shown in Fig. 4(b), the difference between Si-PCPDTBT HOMO and $PC_{60}BM$ LUMO is around 0.6 eV. For $C_{60}$-TH-Hx, the LUMO value is higher around 0.4 eV than that of $PC_{60}BM$. Since the most important factor that determines $V_{oc}$ in BHJ solar cell is the difference between HOMO of donor and LUMO of acceptor, we attribute the increase in $V_{oc}$ obtained with $C_{60}$-TH-Hx to the higher LUMO value of $C_{60}$-TH-Hx.

The external quantum efficiency (EQE) measurement for both Si-PCPDTBT:$C_{60}$-TH-Hx and Si-PCPDTBT:$PC_{60}BM$ solar cells are shown in **Figure 5(c)**. Overall EQE spectrum of Si-PCPDTBT:$PC_{60}BM$ was higher than that of Si-PCPDTBT:$C_{60}$-TH-Hx, consistent with $J_{sc}$ as obtained from the J-V characteristics. To analyze EQE spectra, we also measured absorption spectra of Si-PCPDTBT:$PC_{60}BM$ (1:2, w/w) and Si-PCPDTBT:$C_{60}$-TH-Hx (1:2, w/w) thin films as shown in **Figure 5(d)**. Comparing EQE spectra of devices with absorption spectra of blend films, the photoresponse of devices between 400 nm and 900 nm are similar to the corresponding absorption spectra of each material. However, since absorption intensities of each film are almost identical, the decreased EQE in the Si-PCPDTBT:$C_{60}$-TH-Hx solar cell implies a reduction in the probability of carrier collection.

We have demonstrated BHJ solar cells using Si-PCPDTBT and newly synthesized fullerene derivative, $C_{60}$-TH-Hx with PCE > 4 % (A.M. 1.5 G with 100 mW/cm$^2$). The BHJ solar cell using the $C_{60}$-TH-Hx exhibited higher $V_{oc}$ (0.675 V) and slightly lower $J_{sc}$ in comparison with $PC_{60}BM$ based devices because of more homogeneous phase separation morphology. We anticipate additional improvements in the PCE by further optimizing the morphology of the Si-PCPDTBT:$C_{60}$-TH-Hx system.

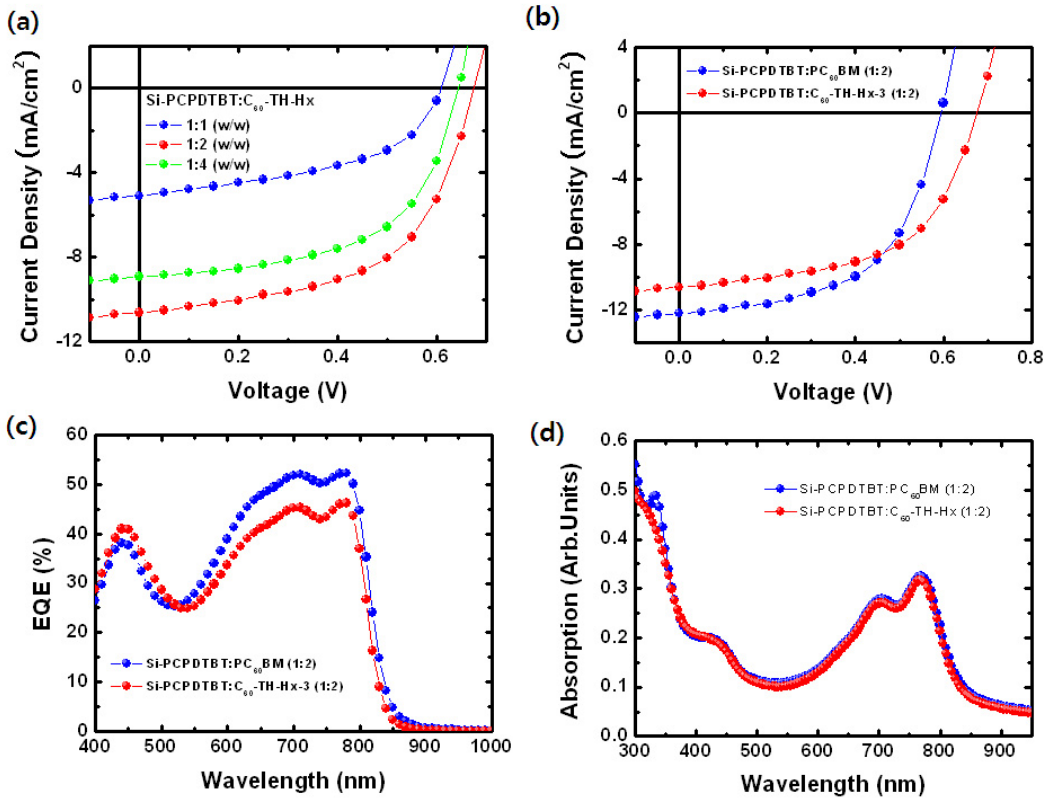


**Figure 5.** (a) Current density-voltage (J-V) characteristics of Si-PCPDTBT:$C_{60}$-TH-Hx solar cell with various ratios, 1:1 (blue filled circle), 1:2 (red filled circle), and 1:4 (green filled circle) under AM 1.5G irradiation with 100 mW/cm$^2$ intensity from calibrated solar simulator. (b) J-V characteristics of Si-PCPDTBT:$PC_{60}$BM and Si-PCPDTBT:C60-TH-Hx devices. (c) External quantum efficiencies spectra of BHJ solar cells fabricated by Si-PCPDTBT:$PC_{60}$BM and Si-PCPDTBT:$C_{60}$-TH-Hx. (d) UV-Vis absorption spectra of Si-PCPDTBT:$PC_{60}$BM (1:2, w/w) and Si-PCPDTBT:$C_{60}$-TH-Hx (1:2, w/w) films. For the Si-PCPDTBT based BHJ solar cells in the literature, $V_{oc}$ was shown around 0.58 V.

### 3) Synthesis and Characterization of Dithienylbenzobis(thiadiazole)-Based Low Band-Gap Polymers.

Benzo[1,2-*c*:4,5-*c*']bis[1,2,5]thiadiazole (BBT) units are known as very strong acceptors due to hypervalent sulfur atoms which can be stabilized in quinoidal structures in a conjugated backbone.[5] In addition, they are expected to have short intermolecular S···N contacts between thiadiazole rings resulted in forming rigid planar geometry of the molecules. Thus BBT derivatives can be utilized for lowering band-gaps in π-conjugated polymers.

We synthesized four new donor-acceptor polymers **PCPBBT**, **PFTBBT** containing BBT as an acceptor group and **PCPBTD**, **PFTBTD** containing benzothiadiazole (BTD) as acceptors and studied their properties. The synthetic schemes for these polymers are shown in **Figure 6.** All polymers showed good solubility in common organic solvents, such as chloroform, chlorobenzene, and toluene. The solubility of the polymers satisfies certain requirement of the fabrication processing for OFET devices. The number-average molecular weights of the polymers were found to be over 10,000.

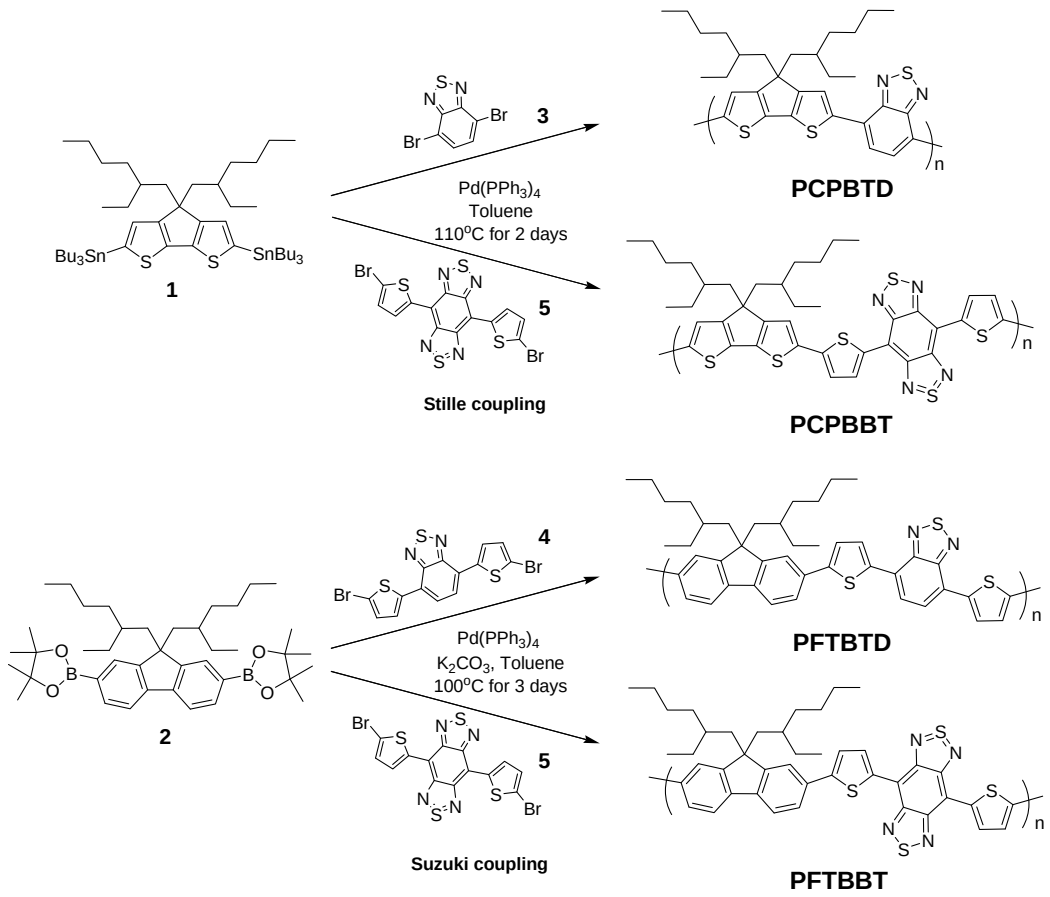


**Figure 6.** The synthetic routes of low band-gap polymers, **PCPBTD**, **PCPBBT**, **PFTBTD**, and **PFTBBT**

Normalized UV/vis characteristics of **PCPBTD**, **PCPBBT**, **PFTBTD**, and **PFTBBT** in chlorobenzene solution and **PCPBBT** in a thin solid film on a glass substrate are summarized in **Table 1**. They all exhibit mainly two absorption bands. The bands in the high energy region are attributed to $\pi$-$\pi^*$ and n-$\pi^*$ transitions of the aromatic segments, and those at longer wavelengths are due to the intramolecular charge transfer (CT) transitions between the donor and acceptor units.

A bathochromic shift was observed by increasing the donor strength from the fluorene to cyclopentadithiophene unit. **PCPBBT** showed highest CT transition absorption at 926 nm red-shifted to 53 nm compared with the absorption of **PFTBBT**. It is noted that although **PFTBTD** has an extended conjugation length from thiophene bridging units, its $\lambda_{max}$ shown at 530 nm is much shorter than that of **PCPBTD** ($\lambda_{max}$ = 702 nm), which contains the cyclopentadithiophene unit. When the BTD unit is replaced by the stronger acceptor, BBT, in the conjugated polymer backbone, significantly large red-shift in the absorption is induced. Compared to the $\lambda_{max}$ for **PFTBTD**, it was found to red-shift with more than 300 nm for **PFTBBT**. This result clearly indicates that the BBT units containing a hypervalent sulfur atom provide enhanced intramolecular CT and effective electronic delocalization leading to a stronger electron-accepting property.

From the cyclicvoltammetry studies the electrochemical band-gaps were found to be 2.05, 1.60, 1.20, and 1.01 for **PFTBTD**, **PCPBTD**, **PFTBBT**, and **PCPBBT**, respectively.These values are consistent with the thin-film optical spectra results estimated from the low energy band edges as 2.00, 1.53, 1.25, and 1.00 eV for **PFTBTD**, **PCPBTD**, **PFTBBT**, and **PCPBBT**, respectively. The LUMOs of **PCPBBT** and **PFTBBT** are much lower than those

of **PFTBTD** and **PCPBTD**, suggesting that **PCPBBT** and **PFTBBT** would be able to work as n-type semiconductors. The combined low LUMO energies and small band-gaps are indicative of the highly electron-deficient and π-conjugated nature of **PFTBBT** and **PCPBBT**.

Top-contact OFETs were fabricated by spin-casting of the polymer solution in chlorobenzene (5 mg/mL) on octadecyl-trichlorosilane treated $n^{++}$-$Si/SiO_2$ (200 nm) substrates. Au source and drain electrodes (50 nm) were deposited on the films by using thermal evaporation under high vacuum. The channel length ($L$) and width ($W$) of the transistors were 50 μm and 2 mm, respectively. OFET device characteristics were measured in a glove box filled with $N_2$. The hole ($\mu_h$) and electron mobility ($\mu_e$) and the threshold voltage ($V_t$) were estimated from the square root of drain current-gate voltage ($I_{ds}^{1/2}$ - $V_{gs}$) plots, according to the standard equation in the saturation regime, $I_{ds} = (W/2L)\mu C_i(V_{gs}-V_t)$, where $I_{ds}$ is the drain current, $C_i$ is the capacitance per unit area of gate dielectric, and $V_{gs}$ is the gate voltage.These values are summarized in **Table 1.**

**Table 1.** Physical and optical properties and OFET characteristics of **PFTBTD**, **PCPBTD**, **PFTBBT**, and **PCPBBT**

| Sample | Mn[a] | Mw[a] | PDI[b] | $\lambda_{max\_sol}$[c] (nm) | $\lambda_{max\_film}$[d] (nm) | HOMO[e] (eV) | LUMO[e] (eV) | $E_g$[e] (eV) | $\mu_h$ ($cm^2/V\cdot s$) | $\mu_e$ ($cm^2/V\cdot s$) | $I_{on}/I_{off}$ |
|---|---|---|---|---|---|---|---|---|---|---|---|
| **PFTBTD** | 30,000 | 37,000 | 1.23 | 390, 531 | 398, 539 | -5.43 | -3.38 | 2.05 | $1.7\times10^{-8}$ | - | $< 10^2$ |
| **PCPBTD** | 12,000 | 28,000 | 2.32 | 407, 702 | 411, 723 | -5.10 | -3.50 | 1.60 | $9.2\times10^{-4}$ | - | $7.1\times10^3$ |
| **PFTBBT** | 4,600 | 11,000 | 2.39 | 436, 873 | 424, 879 | -5.12 | -3.92 | 1.20 | $3.1\times10^{-4}$ | - | $1.5\times10^3$ |
| **PCPBBT** | 27,000 | 44,000 | 1.63 | 428, 926 | 422, 951 | -5.33 | -4.32 | 1.01 | $7.1\times10^{-4}$[f] | $3.3\times10^{-3}$[f] | $\sim 10^2$ |

[a] Determined by GPC with polystyrene as a standard and THF as eluent; number average ($M_n$) and weight average ($M_w$) molecular weight. [b] *PDI* = polydispersity index. [c] Measured in chlorobenzene solution. [d] Measured in a thin solid film on a glass substrate. [e] Determined by cyclic voltammetry (CV). HOMO and LUMO were estimated from onset of CV peaks. [f] Optimal mobilities of the annealed device.

No significant mobility changes were observed after annealing the devices of **PFTBTD**, **PCPBTD**, and **PFTBBT**. Interestingly, the device based on **PCPBBT** showed ambipolar characteristics and increased mobility with increased temperature up to 120°C. **Figure 7(a)** and **(b)** show the transfer characteristics of FET in the plots of drain-source current ($I_{ds}$) versus drain-source voltage ($V_{ds}$) at various annealing temperatures for p-type and n-type of **PCPBBT**, respectively. The ambipolar output characteristics are shown in **Figure 7(c)** and **(d)** in devices annealed at 80°C. For the low gate voltages, the devices showed diode-like curves, which are observed frequently in typical ambipolar transistors. At the high gate voltages, p-type and n-type transistor behavior bigins to appear.

We have successfully synthesized new low band-gap D-A polymers based on the bisthiadiazole unit and characterized their optical and physical properties. Among them, **PCPBBT** showed promising results for the use in ambipolar OFETs with respectable mobilities for p-type and n-type devices. Its hole and electron mobilities were found to be $\mu_h = 7.1 \times 10^{-4}$ cm/Vs and $\mu_e = 3.3 \times 10^{-3}$ cm/Vs after annealed at 120°C and 100°C, respectively. The combination of ambipolar mobility, low band-gap, and broad absorption makes **PCPBBT** very attractive optoelectronic applications possibly including OPVs.

**4. Use of nanoparticles acting as antennas to increase light harvesting**

Due to the electron plasma oscillations existed on the interface between metal and dielectric medium under electromagnetic field excitation, gold nanoparticles could exhibit localized

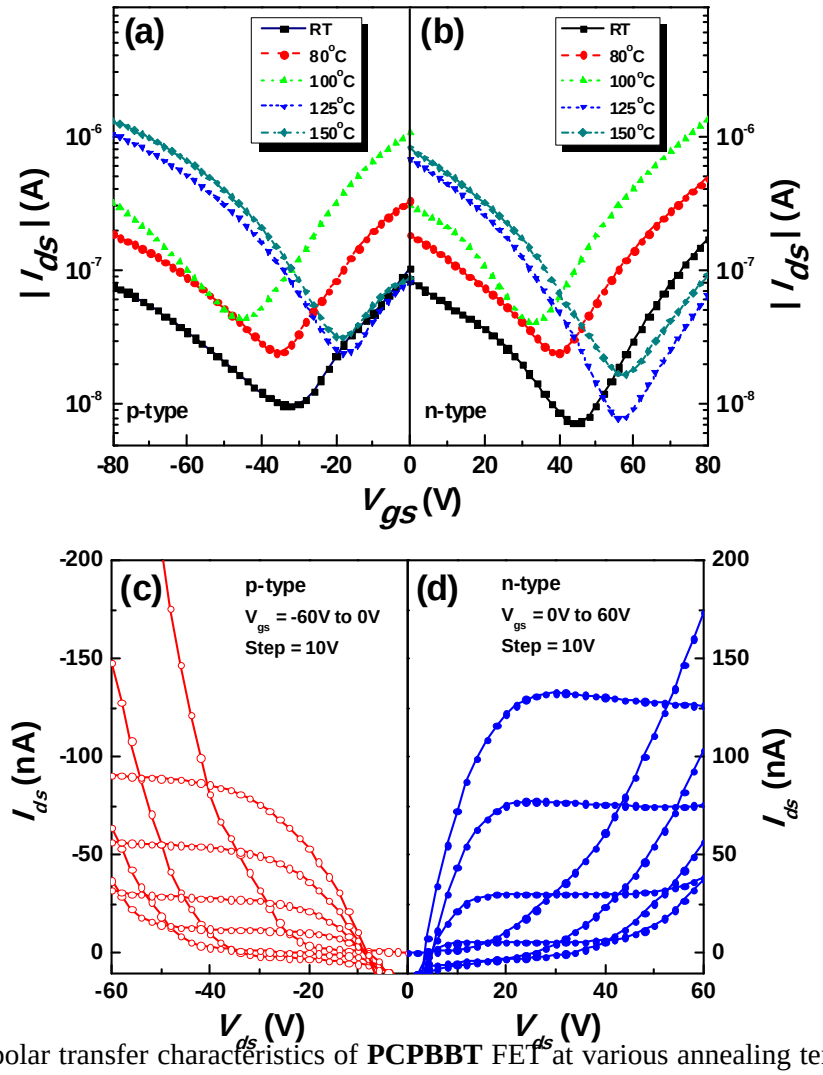


**Figure 7.** Ambipolar transfer characteristics of **PCPBBT** FET at various annealing temperatures; (a) p-type operation mode ($V_{ds}$ = -80 V) and (b) n-type operation mode ($V_{ds}$ = 80 V). $I_{ds}$ versus $V_{ds}$ ambipolar characteristics of **PCPBBT** FET annealed at 80°C for 5 min; (c) p-type operation and (d) n-type operation.

surface plasmon resonance (LSPR) properties. The LSPR effect creates strong near-field electromagnetic fields and far-field propagating waves, which could be used for the enhancement of light absorption of active layer. We have used two type of gold nanospheres (NSs) to study the enhancement of light absorption in organic photovoltaic cells. The larger NS is of diameter 15 nm and the smaller one is 5 nm in diameter as shown in **Figure 8(b).** In a typical device the NSs were dispersed into the anode buffer layer, poly(3,4-ethylenedioxy-thiophene:polystyrenesulfonate) (PEDOT:PSS) (**Figure 8(a)**). The ratio of the NSs could be varied by keeping the other parameters of the device a constant. The phenomenon of LSPR enhancement of light absorption was studied both by simulating the devices and through characterization of fabricated devices. The NSs were found to enhance the performance of the organic photovoltaic cells. Using NSs of 15 nm diameter we could improve the performance of a ITO/PEDOT/MEH-PPV:PCBM/Al cell from 1.99% to 2.36% (**Figure 8(d) & (e)**).

We also found that we can improve the mixing of Au NSs in PEDOT: PSS layer by coating the Au NSs with polyethyleneglycol (PEG-coated-Au). Compared with Au NSs, PEG-coated-Au NSs were much more chemically stable and could disperse better in the PEDOT:PSS layer further improving the of solar cell efficiency. From the EQE measurement of reference device

and devices incorporating PEDOT:PSS doped with various concentrations of PEG-coated-Au NSs solutions, we can see that in the wavelength range from 450 to 600 nm, the photocurrent increased notably after adding the Au NSs. The largest improvement of solar cell efficiency we got at conc. Ax8 was 3.97%. Compared to the original efficiency ($\eta_0$=3.10%), the efficiency of our solar cell was improved about 28% (**Figure 9**).

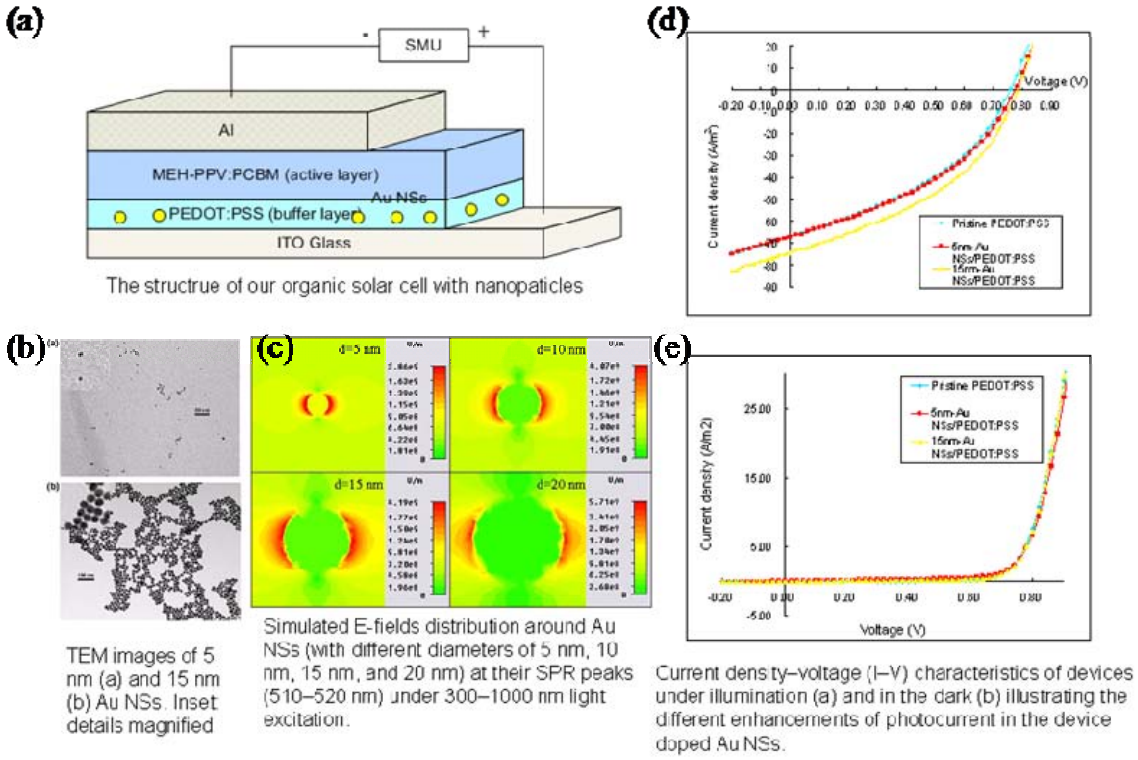


**Figure 8.** Results from the devices that were sensitized by adding Au NSs of 15 nm diameter. (a)Structure of the fabricated device, (b) TEM images of Au NSs, (c) simulations of E-fields around Au NSs with 5, 10, 15 and 20 nm. (d ) & (e) comparison of devices with and without Au NSs.

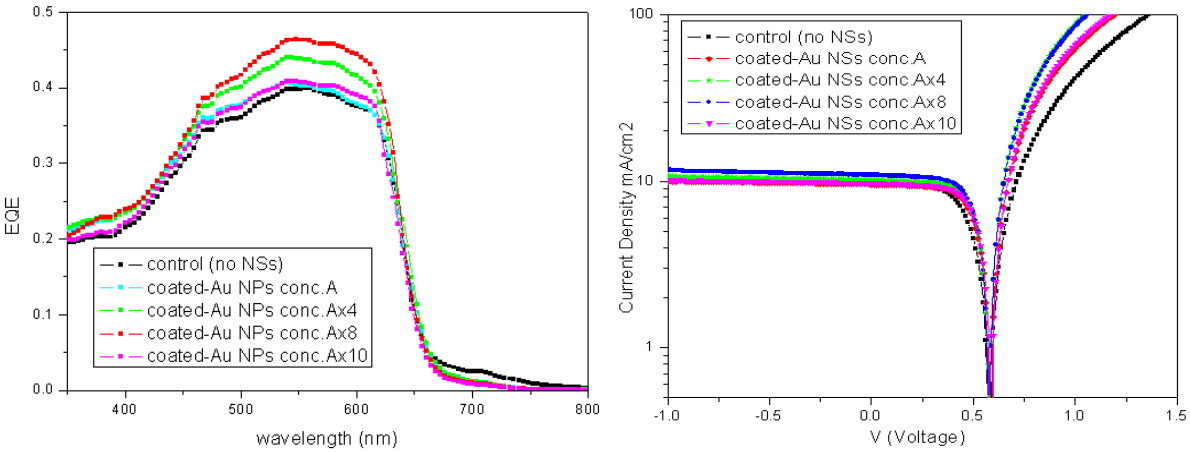


**Figure 9.** EQE measurement (left) and J-V characteristics (right) of different devices incorporating PEDOT:PSS doped with various concentrations of PEG-coated-Au NSs solutions.

## 5. Near infrared light harvesting hybrid solar cell incorporating lead sulfide nanocrystal and low band gap polymer

We fabricated the hybrid photovoltaic solar cell based on the bulk heterojunction of low band gap polymer and lead sulfide (PbS) nanocrystals **(Figure 10).** The low band gap polymer (PDTPBDT) studied in this work showed the absorption maximum of 716 nm in film state with a band gap of 1.4 eV. The oleic acid (OA) ligand-capped PbS nanocrystals with the first exciton wavelength of 920 nm were blended with the polymer to form an energetically favorable type II heterojunction.

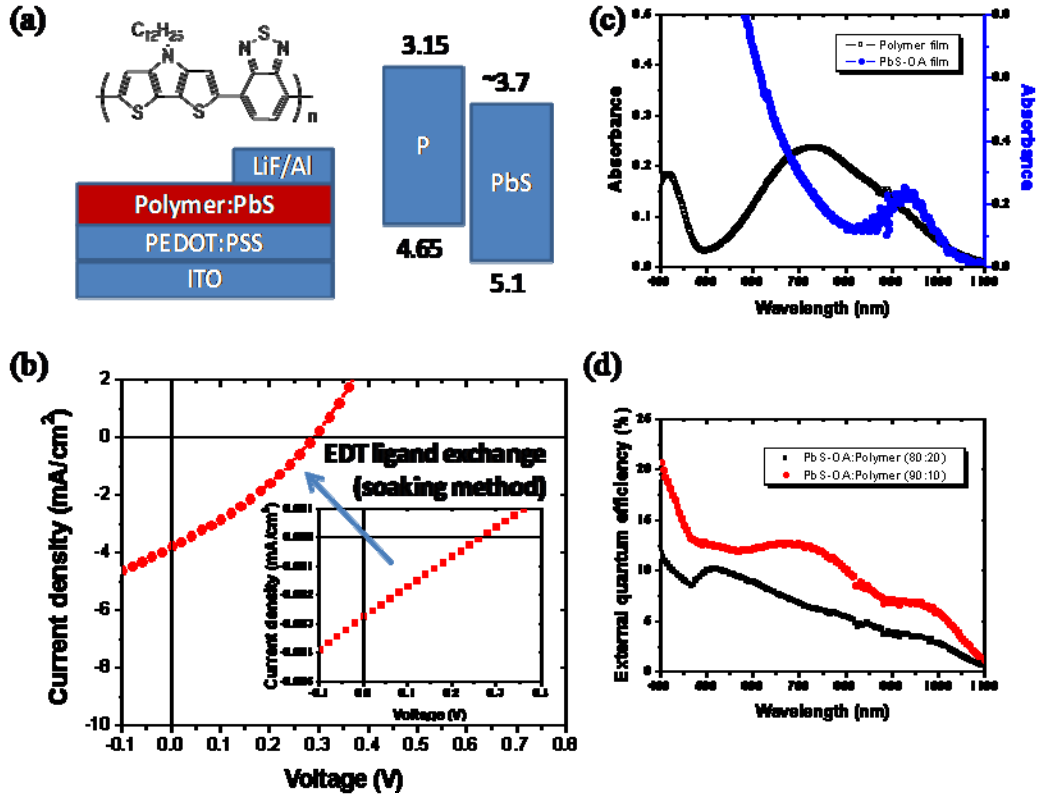


**Figure 10**. (a) Structure of the polymer PDTPBDT, structure of the device fabricated and comparison of the energy levels of PbS and the polymer. (b) I-V characteristics of the device before and after EDT ligand exchange. (c) Comparing the UV-Vis absorption of polymer film and PbS OA film. (d) External quantum efficiency of devices fabricated with different ratios of Pbs-OA: Polymer.

In a hybrid blend film of PbS-OA/polymer (80/20wt%), the photovoltaic performance through post fabrication chemical treatment (soaking method in 1,2-ethanedithiol, EDT solution) was demonstrated to exhibit a $J_{sc}$ of 3.8 mA/cm$^2$, a $V_{oc}$ of 0.29 V, and a FF of 31%. The overall PCE of 0.34% was estimated. In particular, the ligand exchange from OA to EDT resulted in a considerable increase in $J_{sc}$ by ~1350 times due to a better charge transport between the closer packed nanocrystals as well as improved charge generation. Such a photovoltaic performance is confirmed to originate from the both contribution of polymer and PbS nanocrystal by EQE spectra. In the device with PbS-OA/polymer (90/10wt%), more distinctive and apparent responses of polymer and PbS were found to show the broad spectral response in entire wavelength from visible to near infrared (NIR) range. As a result of a preliminary fabrication, we could realize a NIR light harvesting hybrid bulk heterojunction photovoltaic device. Currently, the work on the optimization of fabrication is in progress.

## 4. List of Publications (Total)

1) H. S. Oh, T,-D. Kim, **K.-S. Lee***, S. Cho, **A. N. Cartwright**, **P. N. Prasad***, *Chem. Comm.*, submitted 2010.
*"Synthesis and characterization of dithienylbenzobis(thiadiazole)-based low band-gap polymers for organic electronics".*

2) H. Kim, J. H. Seo, S. Cho*, E. Y. Park, T.-D. Kim, **K.-S. Lee***, K. Lee, A. J. Heeger, *Appl. Phys. Lett.*, 97, 193309 (2010).
*"Increased open-circuit voltage in bulk-heterojunction solar cells using a $C_{60}$ derivative"*

3) J-.J. Park, P. Prabhakaran, K. K. Jang, Y. G. Lee, J. Lee, K. H. Lee, J. Hur, J-.M. Kim*, N. Cho, Y. Son, D.-Y. Yang, **K.-S. Lee***, *Nano Lett.*, **10**, 2310-2317 (2010).
*"Photopatternable quantum dots forming quasi-ordered arrays"*
***-Highlighted by NPG Nature -Asia Materials, Oct. 2010***

4) S. B. Noh, R. H. Kim, W. J. Kim, S. Kim, **K.-S. Lee***, N. S. Cho, H.-K. Shim, H. E. Pudavar, **P. N. Prasad**, *J. Mater. Chem.*, **20**, 7422-7429 (2010).
"Aggregation-enhanced Two-Photon Absorption and Up-converted Fluorescence of Quadrupolar 1,4-bis(cyanostyryl)benzene Derivatives Showing Solvatochromic Fluorescence

5) J. Seo, W. J. Kim, S. J. Kim, **K.-S. Lee**, **A. N. Cartwright,** and **P. N. Prasad***, *Appl. Phys. Lett*., **94,** 133302 (2009).
*"Nanocomposite photovoltaics utilizing CdSe nanocrystals capped with a thermally cleavable Solubilizing ligand"*

6) W. J. Kim, S. J. Kim, **K.-S. Lee,** M. Samoc, **A. N. Cartwright**, and **P. N. Prasad***, *Nano Lett.*, **8(10),** 3262-3265 (2008).
*" Robust Microstructures Using UV Photopatternable Semiconductor Nanocrystals"*
***-Highlighted by SPIE Newsroom, March 26, 2010***

7) J. S. Kim, W. J. Kim, N. Cho, S. Shukla, H. Yoon, J. Jang, **P. N. Prasad**, T.-D. Kim, and **K.-S Lee***, *J. Nanosci. Nanotech.*, **9,** 6957-6961 (2009).
*"Synthesis and properties of Quantum Dot-Polypyrrole Nanotube Composites for Photovoltaic Application"*

8) E. Y. Park, J. S. Park, T.-D. Kim, **K.-S. Lee***, H. S. Lim, J. S. Lim, and C. Lee, *Org. Electron*., **10**, 1028-1031 (2009)
*"High-performanace n-Type Organic Field-Effect Transistors Fabricated by Ink-Jet Printing using a C60 Derivative"*

9) B. Barszcz*, B. Laskowska, A. Graja, E. Y. Park, T.-D. Kim, and **K.-S. Lee**, *Chem. Phys. Lett*., **479**, 224-228 (2009)
*"Vibrational spectroscopy as a tool for characterization of oligothiophene-fullerene linked Dyads"*

10) 1. B. Barszcz*, B. Laskowska, A. Graja, E. Y. Park, T.-D. Kim, **K.-S. Lee**, *Synth. Met.*, **159**, 2539-2543 (2009)
*"Vibrational Properties of Two Fullerene-Thiophene-Based Dyads"*

11) W. J. Kim, S. J. Kim, J. Seo, Y. Sahoo, **A.N. Cartwright, K.-S. Lee, P. N. Prasad**, *Mater. Res. Soc. Symp. Proc.*, **113**, F03-09 (2009)
*"Binding characteristics of surface ligands on PbSe QDs and Impact on Electrical Conductivity"*

12) Y. Cui, **S. He***, *Opt. Lett*., **34(1)**, 16-18 (2009)
*"Enhancing extraordinary transmission of light through a metallic nanoslit with a nanocavity antenna"*

13) N. Cho, K. R. Choudhury, R. B. Theapa, Y. Sahoo, T. Ohulchanskyy, **A. N. Cartwright**, **K-S. Lee*, P. N. Prasad***, *Adv. Mater*., **19**, 232-236 (2007)
"Efficient photodetection at IR wavelengths by incorporation of PbSe-Carbon-Nanotube conjugates in a polymeric nanocomposite",
***-American Chemical Society "Heart Cut" Research Highlight, 2007***

"